Metabolomics and transcriptomics identify pathway differences between visceral and subcutaneous adipose tissue in colorectal cancer patients: the ColoCare study[1,2]

*David B Liesenfeld,[3,10] Dmitry Grapov,[4,10] Johannes F Fahrmann,[4,10] Mariam Salou,[3] Dominique Scherer,[3] Reka Toth,[3] Nina Habermann,[3] Jürgen Böhm,[3] Petra Schrotz-King,[3] Biljana Gigic,[3] Martin Schneider,[5] Alexis Ulrich,[5] Esther Herpel,[6,7] Peter Schirmacher,[7] Oliver Fiehn,[4] Johanna W Lampe,[8,11] and Cornelia M Ulrich[3,8,9,11]**

[3]Division of Preventive Oncology, National Center for Tumor Diseases and German Cancer Research Center, Heidelberg, Germany; [4]NIH West Coast Metabolomics Center and University of California, Davis, CA; [5]Department of General and Transplantation Surgery, University of Heidelberg, Germany; [6]Tissue Bank of the National Center for Tumor Diseases, Heidelberg, Germany; [7]Institute of Pathology, University Hospital Heidelberg, Germany; [8]Cancer Prevention Program, Fred Hutchinson Cancer Research Center, Seattle, WA; and [9]Population Sciences, Huntsman Cancer Institute, Salt Lake City, UT

ABSTRACT

Background: Metabolic and transcriptomic differences between visceral adipose tissue (VAT) and subcutaneous adipose tissue (SAT) compartments, particularly in the context of obesity, may play a role in colorectal carcinogenesis. We investigated the differential functions of their metabolic compositions.

Objectives: Biochemical differences between adipose tissues (VAT compared with SAT) in patients with colorectal carcinoma (CRC) were investigated by using mass spectrometry metabolomics and gene expression profiling. Metabolite compositions were compared between VAT, SAT, and serum metabolites. The relation between patients' tumor stage and metabolic profiles was assessed.

Design: Presurgery blood and paired VAT and SAT samples during tumor surgery were obtained from 59 CRC patients (tumor stages I–IV) of the ColoCare cohort. Gas chromatography time-of-flight mass spectrometry and liquid chromatography quadrupole time-of-flight mass spectrometry were used to measure 1065 metabolites in adipose tissue (333 identified compounds) and 1810 metabolites in serum (467 identified compounds). Adipose tissue gene expression was measured by using Illumina's HumanHT-12 Expression BeadChips.

Results: Compared with SAT, VAT displayed elevated markers of inflammatory lipid metabolism, free arachidonic acid, phospholipases (*PLA2G10*), and prostaglandin synthesis–related enzymes (*PTGD/PTGS2S*). Plasmalogen concentrations were lower in VAT than in SAT, which was supported by lower gene expression of *FAR1*, the rate-limiting enzyme for ether-lipid synthesis in VAT. Serum sphingomyelin concentrations were inversely correlated (P = 0.0001) with SAT adipose triglycerides. Logistic regression identified lipids in patients' adipose tissues, which were associated with CRC tumor stage.

Conclusions: As one of the first studies, we comprehensively assessed differences in metabolic, lipidomic, and transcriptomic profiles between paired human VAT and SAT and their association with CRC tumor stage. We identified markers of inflammation in VAT, which supports prior evidence regarding the role of visceral adiposity and cancer. This trial was registered at clinicaltrials.gov as NCT02328677. *Am J Clin Nutr* 2015;102:433–43.

Keywords: colorectal cancer, obesity, adipose tissue, visceral adiposity, metabolomics, inflammation

INTRODUCTION

Obesity, a condition present in ~30% of colorectal cancer (CRC)[12] patients, has received increasing attention as a prognostic factor with some but not all studies, suggesting worse clinical outcomes associated with excess body weight (1). In addition to energy storage, adipose tissue also acts as a secretory organ involved in the regulation of hormonal and inflammatory pathways (2, 3). Moreover, distinct adipose compartments, visceral adipose tissue (VAT) and subcutaneous adipose tissue (SAT), display differences in anatomic, cellular, and molecular compositions, which may be dependent on the degree of adiposity (4, 5). Unlike SAT, higher concentrations of VAT have been shown to be strongly associated with metabolic dysfunction and related diseases (5, 6).

[1] Supported by NIH grant 1 U24 DK097154 and NIH West Coast Metabolomics Center Pilot Program, German Consortium for Translational Cancer Research, Matthias Lackas Foundation, Division of Preventive Oncology funding, German Cancer Research Center (DKFZ), and Boehringer Ingelheim Fonds and the Helmholtz International Graduate School for Cancer Research. (to DBL).

[2] Supplemental Methods, Supplemental Tables 1–5, and Supplemental Figures 1–3 are available from the "Supplemental data" link in the online posting of the article and from the same link in the online table of contents at http://ajcn.nutrition.org.

[10] These authors contributed equally to this work.

[11] Dual senior authorship.

*To whom correspondence should be addressed. E-mail: neli.ulrich@hci.utah.edu.

[12] Abbreviations used: CRC, colorectal cancer; FDR, false discovery rate; GC-TOF, gas chromatography time of flight; MS, mass spectrometry; PLS-DA, partial least squares discriminant analysis; qTOF, quadrupole time of flight; SAT, subcutaneous adipose tissue; VAT, visceral adipose tissue; VIP, variable importance in projection.

Received December 29, 2014. Accepted for publication June 11, 2015.

First published online July 8, 2015; doi: 10.3945/ajcn.114.103804.

Although evidence linking obesity and CRC is increasing, the underlying biological mechanisms are still unclear. The colon, which is surrounded by mesenteric visceral body fat, has a direct physical and vascular interface with VAT. Given the colon's intimate connection and proximity to visceral fat, we hypothesize that VAT-produced metabolites may have a direct influence on obesity-associated CRC aggressiveness and progression.

Metabolomics has been widely used to characterize biological markers for CRC diagnosis and prognosis and constitutes a powerful tool to probe the biochemistry underlying cancer etiology (7–9). However, previous metabolomic studies of CRC have been mostly limited to the analysis of urine or serum (10).

To date, no study has generated a comprehensive evaluation of the lipidome, metabolome, and transcriptome of human VAT and SAT. In addition, to our knowledge, the impact of compositional differences between adipose tissue compartments on patients' serum metabolic profiles and the relation with cancer stage have never been assessed. The current investigation is one of the first of its kind with regard to the breadth of metabolomic coverage and VAT and SAT profiling to investigate their molecular differences, which may relate to carcinogenesis or prognosis in CRC (11).

METHODS

Study population

This study used specimens from ColoCare—a multicenter, international prospective cohort, recruiting newly diagnosed CRC patients before surgery with the goal to investigate predictors of cancer recurrence, survival, treatment toxicities, and health-related quality of life. Patients (eligibility: newly diagnosed, age 18–80 y, stages I–IV, German speaking, and able to provide informed consent) from the ColoCare Heidelberg cohort were included in this study, recruited between September 2011 and September 2013 at the National Center for Tumor Diseases, Heidelberg, Germany. Patients were staged according to the American Joint Committee on Cancer system based on histopathologic findings. Both colon carcinoma (International Classification of Diseases C18) and rectal or rectosigmoidal cancer patients (International Classification of Diseases C19 or C20) were included. A detailed description of the sample availability and study population is given in **Table 1**. ColoCare has been approved by the ethics committee of the medical faculty at the University of Heidelberg. All study participants provided written informed consent.

Biospecimen collection

Adipose tissue samples (VAT and SAT) from 59 patients (CRC tumor stages I–IV) were obtained during surgery for primary tumor resection. Samples were snap frozen in liquid nitrogen within 45 min and stored at −80°C until further processing. VAT was processed at the tissue bank of the National Center for Tumor Diseases in accordance with the regulations of the tissue bank. VAT was subsequently cut into serial 10-μm aliquots with a total weight of ∼100 mg on a cooled (−25 to −20°C) cryostat (Leica Microsystems), and a representative section was hematoxylin and eosin stained for histopathologic assessment. SAT was manually cut into aliquots within the gas phase of liquid nitrogen. In addition, paired serum samples were collected. Blood was primarily taken 1 d before surgery (n = 48) and, if not possible, intraoperatively (n = 11). Blood samples were processed within 4 h and stored at −80°C until further processing.

Metabolic profiling

For metabolic profiling, all samples were shipped on dry ice to the NIH West Coast Metabolomics Center, University of California, Davis. For gas chromatography time-of-flight (GC-TOF) mass spectrometry (MS) analysis, samples were randomized before analytic analysis by using the Laboratory Information Management System, MiniX (12). For liquid chromatography quadrupole time-of-flight (qTOF) MS analysis, adipose tissue (VAT and SAT) was run as randomized matched patient pairs. Randomization was not blocked for stage, but all samples were analyzed in one batch irrespective of the analytic platform.

Serum and adipose tissue sample preparation

For GC-TOF MS analysis, serum aliquots (30 μL) and adipose tissue (15 mg) were extracted and derivatized as previously described (13). For analysis by ultra-high-performance liquid chromatography-qTOF, 20 μL serum or 5 mg adipose tissue was extracted by using a modified liquid-liquid phase extraction approach by Matyash et al. (14). See **Supplemental Methods** for detailed sample preparation protocols.

GC-TOF MS data acquisition and processing

A Gerstel MPS2 automatic liner exchange system was used to eliminate sample cross-contamination during the GC-TOF MS analysis. Sample (0.5 μL) was injected at 50°C (ramped to 250°C) in splitless mode with a 25-s splitless time. Chromatographic separation was achieved by using an Agilent 7890A gas chromatograph with an Rtx5Sil-MS column (30 m, 0.25 mm inner diameter, 0.25 μm 5% diphenyl film), including an additional 10-m integrated guard column (Restek) (15–17). Chromatographic and mass spectrometric conditions are provided in the Supplemental Methods.

Spectra were processed by using the BinBase database (12, 18). Briefly, output results were filtered based on multiple parameters to exclude noisy or inconsistent peaks (17). All entries in BinBase were matched against the Fiehn mass spectral library of 1200 authentic metabolite spectra by using retention index and mass spectrum information or the National Institute of Standard and Technology 11 library. Metabolites were reported if present in at least 50% of all samples within each group to ensure exclusion of low confidence or background species (19). Data reported as quantitative ion peak heights were normalized by the sum intensity of all annotated metabolites and tissue weight (mg) and used for further statistical analysis.

All samples were analyzed in one batch, throughout which data quality and instrument performance were monitored by using quality control and reference plasma samples (National Institute of Standard and Technology). Quality controls, composed of a mixture of standards analyzed every 10 samples, were monitored for changes in the ratio of analyte peak heights and used to ensure equivalent instrumental conditions over the duration of the data acquisition (13).

Liquid chromatography qTOF MS data acquisition and processing

Lipid extracts were analyzed on an Agilent 1290A Infinity Ultra High Performance Liquid Chromatography system coupled

TABLE 1
Characteristics of the study population (stage I–IV colorectal cancer patients)

	Stage I	Stage II	Stage III	Stage IV	Total
Patients, *n* (%)	9 (15)	23 (39)	16 (27)	11 (19)	59 (100)
Sex, *n* (%)					
Male	7 (16)	16 (37)	14 (33)	6 (14)	43 (73)
Female	2 (12.5)	7 (44)	2 (12.5)	5 (31)	16 (27)
Age, y	62.0 ± 8.4[1]	65.7 ± 12.9	61.6 ± 16.7	59.6 ± 14.7	62.9 ± 13.7
BMI, kg/m^2	27.7 ± 3.3	28.1 ± 4.7	27.5 ± 4.3	24.1 ± 3.7	27.1 ± 4.4
Tumor site, *n* (%)					
Colon	2 (8)	14 (54)	5 (19)	5 (19)	26 (44)
Rectum	7 (21)	9 (27)	11 (34)	6 (18)	33 (56)
Data availability, *n* (%)					
Metabolomics	9 (15)	23 (39)	16 (27)	11 (19)	59 (100)
Transcriptomics	8 (15)	20 (38)	14 (27)	10 (19)	52 (88)

[1]Mean ± SD (all such values).

to an Agilent Accurate Mass-6530-qTOF in both positive and negative modes. Chromatographic and mass spectrometric conditions can be found in the Supplemental Methods. For adipose tissue, 2 injections with different dilution factors were used: *1*) nondiluted extracts were injected at a volume of 5 μL for electrospray ionization ($^{+/-}$), and MS acquisition was captured during the first 8.5 min, before the elution of triglycerides, and *2*) 67.5-fold diluted extracts were injected at a volume of 1 μL to capture mass spectrometric data for triglycerides. Our optimized method for adipose tissue lipidomics enabled us to additionally capture more polar compounds, such as glycerophospholipids (phosphatidylcholines, phosphatidylethanolamines, plasmalogens), sphingomyelins, and ceramides (see **Supplemental Figure 1**). Raw data were processed by using MZmine 2.10 (20), and lipid identification was based on an accurate mass and retention time matching by using internal library databases. In addition, for equivocal identities (i.e., different possible isomers/fatty acid side chains), tandem MS data were used to determine the structural identity. Metabolites that were positively detected at very high mass spectral confidence in at least 5 samples (equal to half the sample size of the smallest stage group) were reported. Data, reported as peak heights for the quantification ion (*m*/*z*) at the specific retention time for each annotated and unknown compound, was normalized to tissue weight (mg) and class-specific internal standard (annotated) or to the internal standard that had the closest retention time (unknowns). Data quality and instrument performance were monitored throughout the data acquisition by using quality controls and pooled reference samples.

Microscopic image analysis

Images of hematoxylin and eosin–stained cryosections of VAT were analyzed by using the Keyence BZ-II analyzer software to measure the mean area (μm^2) of adipocytes in the microscopic image within each section. Area measurements were conducted blinded and independently by 2 different persons to ensure validity.

Gene expression analysis

Adipose tissue sample preparation

For gene expression analysis, whole RNA was extracted from VAT and SAT according to the manufacturer's protocol by using AllPrep DNA/RNA/miRNA Universal Kit (Qiagen). Briefly, ceramic beads were added to fresh-frozen adipose tissue, stored at −80°C, and tissue samples were homogenized by using a Precellys 24 Tissue Lyser (Peqlab). Genomic DNA was separated by binding to DNA spin columns, and flow-through was subsequently used for RNA extraction. Proteins were digested with Proteinase K and removed by chloroform extraction. Remaining DNA was digested by adding DNase I. Pure whole RNA was then obtained by using RNA spin columns. RNA concentration was quantified by using the Epoch Microplate Spectrophotometer (BioTek), and quality was assessed on a Bioanalyzer 2100 (Agilent Technologies). RNA samples that were further analyzed had an RNA integrity number between 6.3 and 9.6.

Gene expression profiling and data processing

Gene expression profiling was performed at the Genomic and Proteomics Core Facilities, German Cancer Research Center, Heidelberg, Germany (21). A total of 200 ng RNA was analyzed by using HumanHT-12 Expression BeadChips (Illumina) according to the manufacturer's instructions. Samples were run in chronological order in which patients received tumor surgery. Paired samples from the same patient (SAT/VAT) were processed in the same batch for most (30/52) samples. Raw data were transformed by using variance-stabilizing transformation and normalized with robust spline normalization. Possible batch effects were adjusted with ComBat (22). All preprocessing steps were carried out in the statistical software R 3.1.0 (www.r-project.org) with the lumi and sva packages (23, 24).

Statistical analysis

Metabolic profiling

Preprocessed data matrices were subject to statistical analyses. We used nonparametrical methods for analyses, because of a deviation from normality for most metabolites. For adipose tissue samples, we compared both a data set that had been normalized only to the respective tissue weight and one that was further normalized to the sum of all metabolite abundances present in the respective chromatogram to get insight into relative concentration ratios within each tissue. Furthermore, data sets were log transformed and autoscaled (25) before statistical analyses.

Univariate analysis

Paired Wilcoxon signed rank tests were used to compare metabolites in VAT with those in SAT of the same patient. Wilcoxon tests were carried out in the freely available software Metaboanalyst 2.0 (26). To test for associations of metabolites in VAT or SAT with patients' tumor stage, we further grouped patients with stages I–II as "early" and III–IV as "late," and we built a logistic regression model in the statistical software R 3.1.0 that accounted for age, sex, BMI, and tumor location as covariates. Metabolites that were associated with stage of disease were further tested for a positive trend with increasing stage (I, II, III, IV) by using Kendall's τ rank correlation with *P* values based on 1000-fold permutation of the stage variable. Spearman rank correlation analyses were carried out between serum and adipose tissue metabolites to assess possible serum metabolites for their use as surrogate markers for adipose tissue biochemistry. Finally, in case of multiple testing, raw *P* values were adjusted by using the Benjamini-Hochberg false discovery rate (FDR) (27). Raw *P* values will be reported as "*P*" in the tables and throughout the text, whereas FDR-corrected *P* values will be reported as "FDR" hereafter.

Multivariate analysis

A partial least squares discriminant analysis (PLS-DA) model for the comparison of metabolites in VAT and SAT was calculated in Metaboanalyst 2.0. To test for possible overfitting, 10-fold cross-validation was applied within the build-in PLS-DA toolbox of Metaboanalyst 2.0. The robustness of the class separation was assessed by permutation testing (2000-fold permutation of the group label). PLS-DA model variable importance in projection (VIP) values were calculated and used to identify importantly altered metabolites during biochemical network analysis (see Network visualization section below).

Network visualization

Network mapping (28) was used to interpret statistical and multivariate results within a biological context. A biochemical and chemical similarity network was constructed between all measured and annotated metabolites. MetaMapR (https://github.com/dgrapov/MetaMapR) was used to identify metabolic precursors to product relations based on Kyoto Encyclopedia of Genes and Genomes identifiers (29). PubChem chemical identifiers (https://pubchem.ncbi.nlm.nih.gov/) were used to calculate structural similarities. Molecular fingerprints were compared and a threshold for structural similarity was defined at a Tanimoto coefficient >0.7. Lipid species with ambiguous structural or biochemical information were connected based on the similarity in the complex lipid class (triglyceride, diacylglyceride, phosphoglycerolipid, sphingomyelin/ceramide). Network node properties, representing metabolites, were defined based on statistical and multivariate modeling results.

Integrating gene expression data

For the integration of gene expression data, we used our metabolomics data set to target the transcriptomic analyses. Genes encoding for enzymes of metabolic pathways covered with our metabolic profiling approach were extracted by using KEGG (29) (see **Supplemental Table 1** for a subset of genes). Paired Wilcoxon signed rank tests were used to compare gene expression patterns in VAT with those in SAT of the same patient. We carried out pathway enrichment analyses for both the metabolomic and the transcriptomic data set. For metabolite data, a metabolite set enrichment analysis was carried out in Metaboanalyst 2.0 by using the standard pathway-associated metabolite set. For the gene expression data set, we carried out significance analysis of functional categories in gene expression analysis (30) by using the R-package "safe" (31) and gene sets from the REACTOME database (32). To illustrate the direct agreement between the metabolomic and transcriptomic data sets, we calculated Spearman rank correlations between gene expression and metabolite concentrations for every gene in both SAT and VAT. The most important and consistently observed correlations in both tissues can be found in **Supplemental Table 2**.

RESULTS

Metabolomics

Metabolite coverage

Metabolomic measurements of primary metabolites and complex lipids in paired biospecimens (VAT, SAT, and serum) from 59 CRC patients were carried out by using a combination of GC-TOF MS and liquid chromatography qTOF MS platforms. A total of 1810 metabolites were detected in serum; 467 of those could be annotated. Similarly, 1065 metabolites were detected in adipose tissues, and 333 of those were annotated.

Metabolic differences between VAT and SAT

Independent of the metabolomic data normalization method used, there were marked differences in the metabolomic profiles between VAT and SAT. Metabolomic network analysis and mapping (**Figure 1**) were used to visualize global differences between the 2 adipose compartments. Statistical and multivariate results for all metabolites with PLS-DA model VIP >1.5 are summarized in **Table 2**. Our PLS-DA model did not show any signs of possible overfitting, as indicated by cross-validation. Moreover, none of the permuted models performed better than the original model in separating classes.

Differences in primary metabolism and free fatty acids

Compared with SAT, VAT displayed higher abundances of most measured amino acids, nucleosides, and carbohydrate metabolites (Figure 1, left). Only select sugars and sugar alcohols (glucose, fucose, mannose, and galactitol; all FDR <0.05) showed marginally lower abundances in VAT compared with SAT (Figure 1). With the exception of arachidonic acid, most free fatty acids were lower in VAT. Interestingly, arachidonic acid was consistently elevated (FDR = 7.3×10^{-7}) in VAT compared with SAT among 52 of 59 paired comparisons (Figure 1). The difference in arachidonic acid between VAT and SAT also constituted one of the most important multivariate discriminant metabolites (PLS-DA VIP $>$ 2.5) between these 2 adipose depots.

Differences in complex lipid metabolism

Numerous complex lipids were altered between the 2 adipose compartments. In particular, all measured ceramides were elevated in VAT compared with SAT (all FDR <0.01). In contrast to ceramides, most sphingomyelin lipids were lower in VAT (Figure 1, bottom).

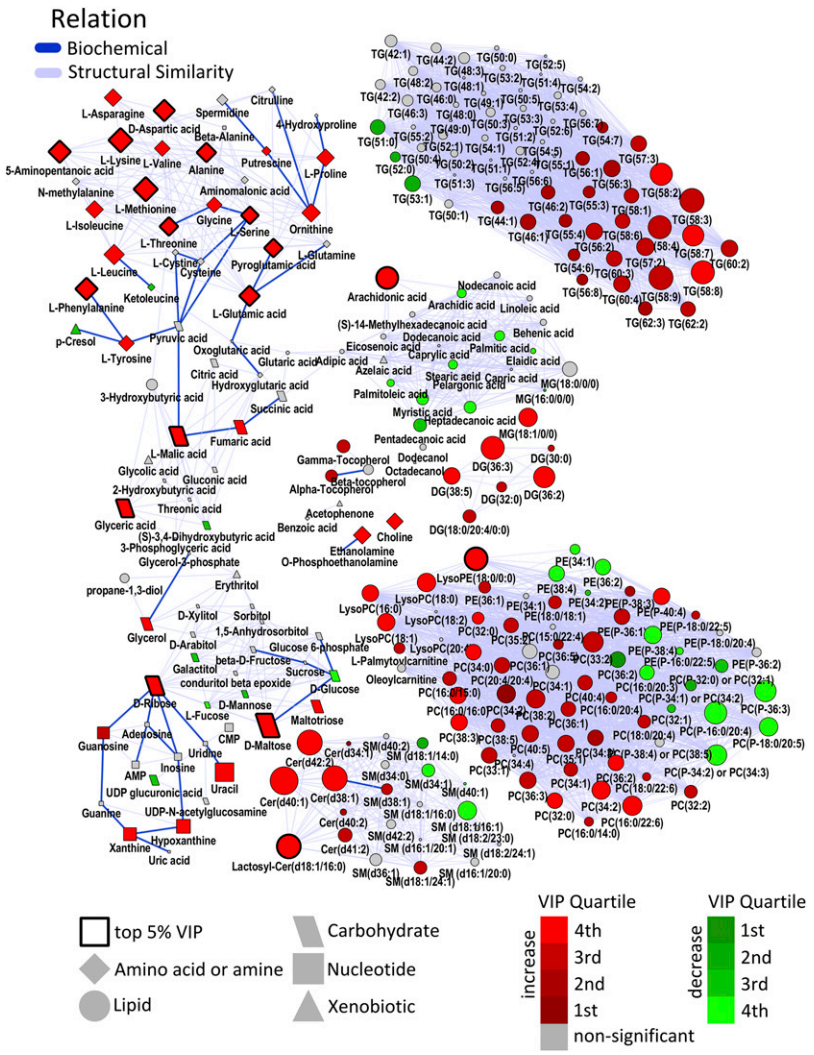

FIGURE 1 Biochemical and structural similarity network displaying metabolic differences between SAT and VAT. Network nodes representing metabolites (shape displaying the biochemical domain) are connected based on biochemical (precursor to product, blue lines) or structural similarity (Tanimoto > 0.07, gray lines) or complex lipid class–specific relations (gray lines). The direction of the metabolic differences in VAT relative to SAT tissue (green, lower in VAT; red, higher in VAT, gray; inconclusive or FDR-adjusted $P \geq 0.05$) is defined based on the number of matched samples (≥30) displaying the trend. The multivariate importance of the metabolomic differences for discriminating between VAT and SAT tissues is displayed based on the color brightness, which encodes the quartile for the partial least squares discriminant analysis VIP, with thick black borders displaying species with the top 5% VIP values. Node size is proportional to the number of higher/lower pairs (30 times out of 59 pairs lower/higher = small size, 59 times or 0 times higher/lower = big size). Cer, ceramide; DG, diacylglycerol; FDR, false discovery rate; MG, monoacylglycerol; PC, phosphatidylcholine; PE, phosphatidylethanolamine; SAT, subcutaneous adipose tissue; SM, sphingomyelin; TG, triacylglycerol; VAT, visceral adipose tissue; VIP, variable importance in projection.

Higher molecular weight triglycerides, with a mean of 56 carbons and 4 double bonds, were elevated in VAT compared with SAT, whereas lower molecular weight triglycerides with fewer double bonds (51 carbons, 3 double bonds) remained unchanged between the 2 compartments (Figure 1, top right).

VAT and SAT showed distinct differences in glycerophospholipids (Figure 1, bottom right). Most phosphatidylcholines and phosphatidylethanolamines were higher in VAT than in SAT. Lysoglycerophospholipids (containing one fatty acid, lysophosphatidylcholines, and lysophosphatidylethanolamine) were also markedly higher in VAT. In particular, a stearic acid containing lysophosphatidylethanolamine (18:0) was among the most important metabolites discriminating VAT from SAT (top 5% based on VIP values in the PLS-DA). In contrast, plasmenyl-phospholipids and select phosphatidylethanolamines with higher degrees of unsaturation and specifically those containing arachidonic acid [i.e., Figure 1: phosphatidylcholine (P-16:0/20:4); FDR = 6.8×10^{-8}] were reduced in VAT compared with SAT.

Correlations between serum and adipose tissue metabolites

Sampling adipose tissue (especially VAT) is an invasive procedure. We therefore probed empirical associations between the easily accessible serum metabolites and adipose tissue metabolites. In general, serum metabolites showed a low degree of correlation with their SAT and VAT localized counterparts. This is not unexpected given that serum metabolite compositions constitute the sum integrated pool of metabolites from all organismal tissues and exogenous sources. Although the correlation between total adipose tissue and serum triglycerides was low (see **Supplemental Figure 2**, top), we did observe moderate correlations

TABLE 2
Summary of the most significantly different metabolites between SAT and VAT based on a PLS VIP value (component 1) >1.5 and an FDR <0.05[1]

Metabolite ID	Match	$N\uparrow$ in VAT[2]	HMDB ID	SAT[3]	VAT[3]	FC[4]	P[5]	FDR[6]	PLS VIP[7]
Plasmenyl-PC (34:2)	PC [P-16:0/18:2(9Z,12Z)]	7	11211	4756 ± 1735	2770 ± 1020	0.6	8.7×10^{-11}	3.0×10^{-9}	2.11
Cer (d38:1)	Ceramide (d18:1/20:0)	54	04951	4591 ± 1222	6144 ± 1638	1.3	1.6×10^{-10}	3.0×10^{-9}	1.51
Ceramide (d40:1)	Ceramide (d18:1/22:0)	57	04952	18,309 ± 5953	26,036 ± 6520	1.4	1.1×10^{-10}	9.8×10^{-9}	2.04
Lactosylceramide (d18:1/16:0)	Lactosylceramide (d18:1/16:0)*	54	06750	10,029 ± 20,705	27,756 ± 35,517	2.8	5.4×10^{-10}	2.5×10^{-8}	2.11
DG (36:3)	DG (18:0/0:0/18:3n–6)	52	56049	100,168 ± 63,102	194,375 ± 159,245	1.9	9.1×10^{-10}	3.3×10^{-8}	1.62
LPE (18:0/0:0)	LPE (18:0/0:0)	53	11130	1068 ± 746	6214 ± 12,508	5.8	1.5×10^{-9}	3.8×10^{-8}	2.06
Maltose	D-maltose	54	00163	1090 ± 1070	4086 ± 3494	3.7	5.2×10^{-10}	6.0×10^{-8}	3.07
Lysine	L-lysine	54	00182	4550 ± 2488	9049 ± 5334	2.0	9.0×10^{-10}	6.0×10^{-8}	2.53
Plasmenyl-PC (36:4)	PC [P-16:0/20:4(5Z,8Z,11Z,14Z)]*	5	11220	4793 ± 2536	2250 ± 993	0.5	5.5×10^{-9}	6.8×10^{-8}	2.16
Methionine	L-methionine	54	00696	705 ± 455	1747 ± 1495	2.5	1.7×10^{-9}	7.6×10^{-8}	2.71
Ceramide (d42:2)	Cer [d18:1/24:1(15Z)]	54	04953	24,660 ± 9440	36,461 ± 12,759	1.5	5.5×10^{-9}	1.1×10^{-7}	1.89
Phenylalanine	L-phenylalanine	52	00159	2767 ± 1441	5280 ± 3018	1.9	5.8×10^{-9}	1.9×10^{-7}	2.49
Plasmenyl-PE (36:4)	PE [P-16:0/20:4(5Z,8Z,11Z,14Z)]*	11	08937	14,258 ± 4288	9951 ± 2541	0.7	2.7×10^{-8}	2.5×10^{-7}	1.97
DG (36:2)	DG (18:0/0:0/18:2n–6)	50	56048	180,426 ± 94,977	304,989 ± 180,447	1.7	2.2×10^{-8}	3.1×10^{-7}	1.69
Malic acid	L-malic acid	49	00156	735 ± 387	1218 ± 415	1.7	2.0×10^{-8}	5.4×10^{-7}	2.67
5-Aminovaleric acid	5-Aminopentanoic acid	52	03355	158 ± 61	525 ± 549	3.3	2.8×10^{-8}	5.6×10^{-7}	2.77
Glutamic acid	L-glutamic acid	50	00148	4729 ± 2435	8936 ± 5681	1.9	2.9×10^{-8}	5.6×10^{-7}	2.27
Aspartic acid	L-aspartic acid	51	00191	2645 ± 1051	5732 ± 3418	2.2	4.4×10^{-8}	6.5×10^{-7}	2.68
Histidine	L-histidine	50	00177	878 ± 516	1655 ± 1093	1.9	4.4×10^{-8}	6.5×10^{-7}	2.19
Arachidonic acid	Arachidonic acid	52	01043	937 ± 350	3645 ± 4651	3.9	5.5×10^{-8}	7.3×10^{-7}	2.70
Oxoproline	Pyroglutamic acid	48	00267	32,556 ± 17,603	58,826 ± 41,557	1.8	6.3×10^{-8}	7.6×10^{-7}	2.12
PC (p-38:5) or PC (o-38:6)	PC [P-18:0/20:5(5Z,8Z,11Z,14Z,17Z)]*	12	11255	38,326 ± 20,286	22,824 ± 11,941	0.6	6.6×10^{-8}	8.2×10^{-7}	1.68
Threonine	L-threonine	48	00167	3351 ± 1485	5286 ± 2299	1.6	9.8×10^{-8}	1.1×10^{-6}	2.32
Plasmenyl-PE (38:5)	PE [P-18:0/20:5(5Z,8Z,11Z,14Z,17Z)]	12	11387	5915 ± 2210	4226 ± 1368	0.7	1.8×10^{-7}	1.1×10^{-6}	1.66
Serine	L-serine	47	00187	7826 ± 3021	12,071 ± 4843	1.5	1.2×10^{-7}	1.2×10^{-6}	2.27
Ribose	D-ribose	49	00283	253 ± 115	485 ± 272	1.9	1.4×10^{-7}	1.3×10^{-6}	2.55
PC (p-36:4) or PC (o-36:5)	PC [P-16:0/20:4(5Z,8Z,11Z,14Z)]*	8	11220	186,360 ± 78,351	116,539 ± 61,169	0.6	1.3×10^{-7}	1.4×10^{-6}	1.69
Plasmenyl-PC (36:3)	PC [P-18:0/18:3(6Z,9Z,12Z)]	9	11245	10,371 ± 6471	6516 ± 3355	0.6	2.8×10^{-7}	2.7×10^{-6}	1.51
Leucine	L-leucine	49	00687	11,005 ± 6258	18,898 ± 11,843	1.7	4.7×10^{-7}	4.2×10^{-6}	2.00
Alanine	L-alanine	49	00161	31,118 ± 13,343	46,593 ± 17,858	1.5	6.1×10^{-7}	5.0×10^{-6}	2.17
Ornithine	Ornithine	47	00214	2523 ± 939	3863 ± 1999	1.5	8.7×10^{-7}	6.8×10^{-6}	2.02
LPC (18:0)	LPC (18:0)	47	10384	8691 ± 6947	37,476 ± 130,402	4.3	9.1×10^{-7}	7.0×10^{-6}	1.55
Glyceric acid	Glyceric acid	48	00139	521 ± 202	835 ± 423	1.6	1.2×10^{-6}	8.9×10^{-6}	2.20
SM (d18:1/16:1)	SM (d18:1/16:1)	12	NA	47,232 ± 18,983	33,286 ± 17,280	0.7	1.3×10^{-6}	9.1×10^{-6}	1.55
LPC (16:0)	LPC (16:0)	45	10382	17,484 ± 16,639	86,936 ± 323,719	5.0	2.6×10^{-6}	1.7×10^{-5}	1.52
Tyrosine	L-tyrosine	44	00158	4529 ± 2225	7167 ± 3889	1.6	2.9×10^{-6}	2.0×10^{-5}	1.86
Isoleucine	L-isoleucine	46	00172	6127 ± 2821	9148 ± 4938	1.5	4.7×10^{-6}	3.2×10^{-5}	1.81
Proline	L-proline	46	00162	7410 ± 4602	11,255 ± 6499	1.5	9.3×10^{-6}	5.9×10^{-5}	1.81
Uracil	Uracil	47	00300	419 ± 237	700 ± 457	1.7	1.1×10^{-5}	6.5×10^{-5}	1.91
Valine	L-valine	44	00883	14,113 ± 7790	19,454 ± 10,157	1.4	4.4×10^{-5}	2.6×10^{-4}	1.56
Maltotriose	Maltotriose	41	01262	195 ± 109	330 ± 224	1.7	3.6×10^{-4}	0.002	1.55
Fumaric acid	Fumaric acid	42	00134	636 ± 265	836 ± 352	1.3	0.001	0.002	1.66
Xanthine	Xanthine	41	00292	222 ± 87	306 ± 142	1.4	0.001	0.004	1.74

[1]Match in the HMDB: for complex lipid species, matches are putative, based on the population in the HMDB. Fatty acid side chains were confirmed by using tandem mass spectrometry for matches indicated by asterisks (*). DG, diacylglycerol; FC, fold change; FDR, false discovery rate; HMDB, human metabolome database; LPC, lysophosphatidylcholine; LPE, lysophosphatidylethanolamine; PC, phosphatidylcholine; PE, phosphatidylethanolamine; PLS, partial least squares; SAT, subcutaneous adipose tissue; SM, sphingomyelin; VAT, visceral adipose tissue; VIP, variable importance in projection.

[2]Number of elevated pairs in VAT. Example: the metabolite was higher in VAT in 49 of 59 matched pairs for $N\uparrow = 49$.

[3]Values are means ± SDs of the raw mass spectrometric intensities, normalized to the total metabolic intensity signal.

[4]Positive values indicate higher abundances in VAT; negative values indicate higher abundances in SAT.

[5]Raw P value from matched Wilcoxon rank sum tests.

[6]FDR-corrected P value.

[7]VIP value of the first principal component in a PLS discriminant analysis.

(Spearman r = 0.25–0.35) between selected serum and SAT triglycerides. We expanded correlation analyses between different lipid species in adipose tissue and serum. Surprisingly, we identified statistically significant inverse correlations between total serum sphingomyelins and SAT triglycerides (FDR = 0.0001; see **Supplemental Table 3** for a list of metabolites).

This correlation was not observed between VAT triglycerides and serum sphingomyelins (see also Supplemental Figure 2, bottom).

Adipose tissue metabolites associated with CRC tumor stage

Logistic regression was used to test for differences in metabolite concentrations in VAT or SAT between early (stages I–II) and late (stages III–IV) CRC tumors with adjustment for tumor location and patients' age, sex, and BMI. None of the tested metabolites remained significant after multiple test correction. However, some lipids showed moderate trends with CRC tumor stage, indicated by Kendall's τ correlation (see **Supplemental Table 4**). **Figure 2**A illustrates lipids with raw $P < 0.05$ for both logistic regression and Kendall's τ correlation with $\tau > 0.25$ or $\tau < -0.25$ in VAT. These species were low abundant lipids that were missed in data-dependent tandem MS fragmentation during data acquisitions, rendering these compounds nonannotated. Comparison of accurate masses and retention times to known lipids did not yield hits with <5 ppm mass error.

Association between age, sex, BMI, and adipose metabolic profiles

Multiple linear regression models were used to test associations between SAT and VAT metabolite concentrations and patients' age, sex, and BMI. No measured species were significantly associated with patients' sex after adjusting for multiple testing. Only 5 metabolites, triglycerides (58:8; 56:7, 56:8, and 58:7) and phosphatidylcholine (P-36:3), were significantly associated with patients' age (FDR = 0.03–0.05). However, we did

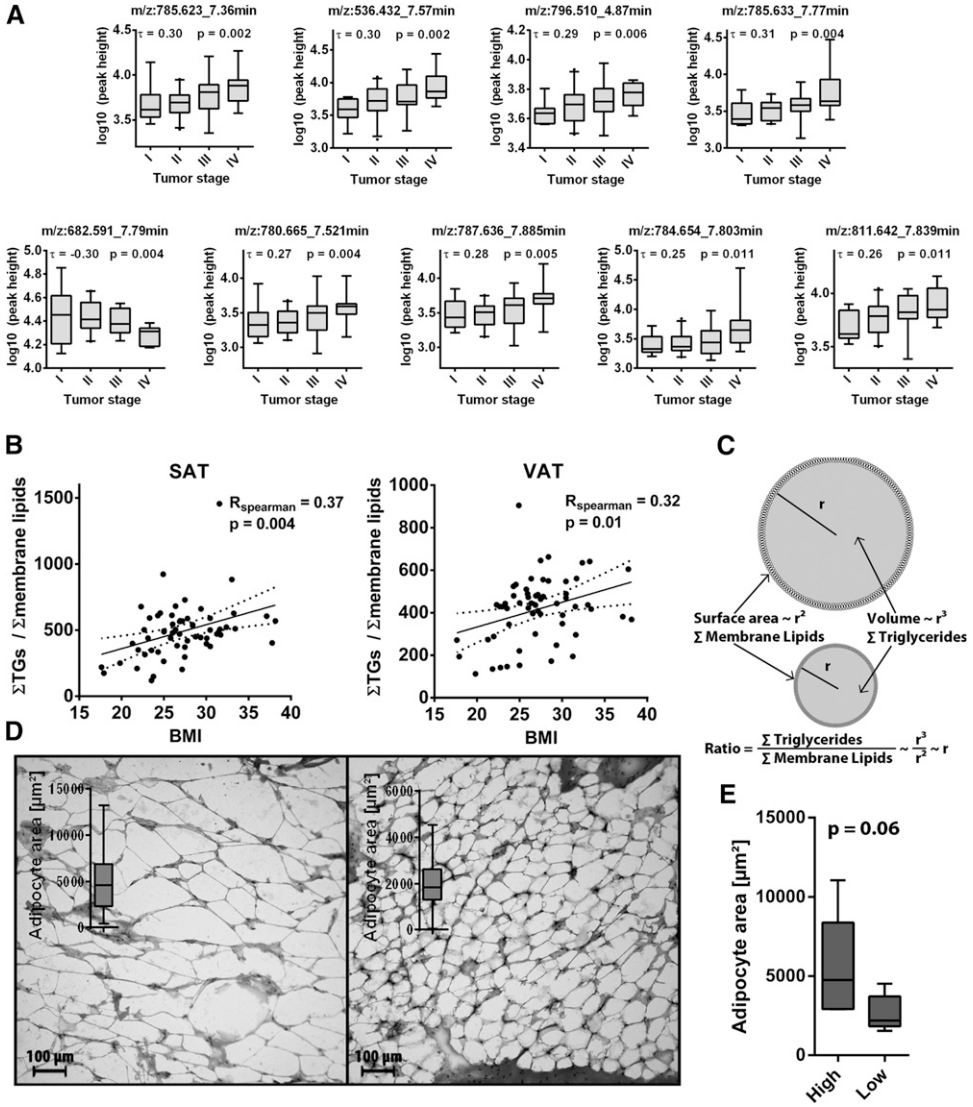

FIGURE 2 Association between the adipose tissue metabolome with tumor stage and BMI. (A) Box-whisker plots for normalized peak heights of unknown lipid species in VAT for which a trend was observed with increasing tumor stage. *P* values are based on Kendall's τ correlation with 1000-fold permutation analysis of the stage variable to account for ties. Detected lipids are marked by accurate mass and chromatographic retention time. (B) Positive association between the ratio of triglycerides/membrane lipids and patients' BMI in both SAT (left) and VAT (right) indicating (C) increased adipocyte diameter with increasing BMI. (D) Representative microscopic images of hematoxylin and eosin–stained cryosections of VAT from a patient with a high triglyceride/membrane lipid ratio (left) and a low triglyceride/membrane lipid ratio (right). (E) Box-whisker plot representing the adipocyte area in those patients with the top 5 highest triglyceride/membrane lipid ratios compared with those patients with the lowest 5 triglyceride/membrane lipid ratios; *P* value derived from Wilcoxon signed rank test. SAT, subcutaneous adipose tissue; TG, triacylglycerol; VAT, visceral adipose tissue.

observe an interesting pattern related with BMI. Concentrations of high-molecular-weight SAT triglycerides (carbon numbers 56–58; double bonds 6–8) were positively correlated with BMI (FDR = 0.005–0.025). In contrast, select phospholipids (phosphatidylcholines and one phosphatidylethanolamine) showed an inverse correlation with BMI (see **Supplemental Table 5**). On the basis of this observation, we calculated the ratio between total triglycerides and membrane lipids [triglycerides / (phosphatidylcholines + phosphatidylethanolamines + plasmalogens + sphingomyelins + ceramides)], which was positively correlated with patients' BMI in both SAT and VAT (see Figure 2B), indicating that BMI was positively associated with adipocyte cell size (see Figure 2C). Subsequently, we measured the area of adipocytes in VAT of 10 patients based on their triglyceride/membrane lipid ratio (top 5 compared with lowest 5) and observed a larger adipocyte size ($P = 0.06$) in patients with the high ratio (see Figure 2D and 2E and **Supplemental Figure 3**).

Gene expression analysis

Transcriptomic analysis was used to confirm the observations from the metabolomic investigations. We analyzed differences in gene expression between VAT and SAT for enzyme-encoding genes that were part of metabolic pathways covered by our metabolomics approach (see Supplemental Table 1). Correlations between gene expression and metabolite concentrations generally indicated a positive and complementary agreement in the description of cellular biochemical processes (see Supplemental Table 2). Positive correlations of various triglycerides with *CLYBL* (citrate lyase β-like) underlined the role of citrate lyase in lipogenesis, whereas negative correlations between the amino acids valine, lysine, and leucine with *ALDH9A1* correspond to the role of this aldehyde dehydrogenase in the shared oxidative pathway of these amino acids (29).

Results of pathway enrichment analyses (metabolomics compared with transcriptomics) are given in **Table 3**. The fundamentally different metabolisms of VAT compared with SAT were confirmed by our metabolite set enrichment analysis, indicated by many significantly overenriched pathways. In contrast, the top 10 overenriched pathways in our transcriptomic analysis did not reach significance after FDR correction. However, the most enriched pathway in the transcriptomic data set was the "synthesis of prostaglandins and thromboxanes" ($P = 0.004$), a finding that particularly confirmed the arachidonic acid pathway of our metabolomics data set.

Arachidonic acid metabolism

Gene expression was elevated in VAT compared with SAT for many arachidonic acid metabolism-related enzymes, specifically phospholipases (*PLA2G10*, FDR = 1.0×10^{-4}), prostaglandin synthase D (*PTGDS*, FDR = 1.7×10^{-7}), and prostaglandin synthase 2 (*PTGS2* also known as *COX2*, probe 1: FDR = 2.2×10^{-5}, probe 2: FDR = 2.7×10^{-5}; see also Supplemental Table 1). These findings align with our initial observation of significantly elevated arachidonic acid in VAT. **Figure 3** displays the results of the combined transcriptomic and metabolomic analysis for the arachidonic acid pathway. In addition to higher expression of selected *PLA2*s, lower abundances of their educts were detected in VAT, specifically for some phosphatidylethanolamines as well as plasmenyl species. Notably, phosphatidylethanolamine (38:4), putatively phosphatidylethanolamine (20:4/18:0), and lysophosphatidylethanolamine (18:0) displayed an inverse educt-product relation (see Figure 3, top).

Plasmalogen synthesis

Metabolomic analysis indicated overall lower abundances of ether lipids (plasmalogens) in VAT compared with SAT. Consistent with this observation, gene expression of fatty acyl reductase 1 (*FAR1*), the rate-limiting enzyme for ether lipid synthesis, was significantly reduced in VAT compared with SAT (fold change = 0.85; FDR = 1.2×10^{-5}).

Ceramide and sphingolipid metabolism

We observed lower concentrations of selected sphingomyelins in conjunction with higher abundances of ceramides in VAT compared with SAT. Although these changes constituted some of the major differences in lipids between these 2 tissues (see Table 2), gene expression for sphingomyelinases (*SMPD1–4*) or sphingomyelin synthases (*SGMS1, SGMS2*) was similar between VAT and SAT.

DISCUSSION

VAT is metabolically different from SAT

Compared with SAT, VAT displayed higher abundances for most metabolites involved in primary metabolism (e.g., amino acids, nucleotides, carbohydrates, and organic acids; see Figure 1, left), suggesting that this adipose depot is more metabolically active. These findings support previous evidence that has characterized VAT as an active endocrine organ with complex roles beyond energy storage. In contrast, almost all free fatty acids, with the exception of arachidonic acid, were elevated in SAT, indicating that SAT may be more active with regard to lipid storage and release, the latter of which may be accelerated during surgery (33). Adipose compartment–specific differences in phospholipids may be related to differences in phospholipase expression and activity, particularly *PLA2*, between the 2 tissues. A similar case can be made for plasmalogens, the majority of which were lower in VAT relative to SAT (see Figure 1, bottom right). Changes in these complex lipids were directly supported by lower expression of *FAR1*, the rate-limiting enzyme for ether-lipid synthesis (34), in VAT compared with SAT.

Plasmalogens' biological roles and implications in health and disease have been widely studied (35, 36). It has been speculated that one of the primary roles of plasmalogens is for sequestration of unsaturated fatty acids such as arachidonic acid (36) for lipid signaling. Depleted plasmalogen abundances in VAT compared with SAT may indicate higher phospholipase A2–dependent lipid signaling activity in VAT. However, because of lack of detection of lysoplasmalogens, altered de novo plasmalogen synthesis between the 2 tissues cannot be ruled out as a possible source of disparity for these lipids between VAT and SAT.

Patients' BMI is a predictor of the adipose triglyceride to membrane lipid ratio

Abundances of select SAT triglyceride and phospholipid species were directly dependent on BMI. Specifically, the ratio between triglycerides and membrane lipids was significantly

TABLE 3
Ten most significantly enriched metabolic pathways in the metabolomics/lipidomics and gene expression data sets comparing VAT with SAT[1]

Metabolomics			Transcriptomics		
Pathway	*P*	FDR	Pathway	*P*	FDR
Betaine metabolism	1.0×10^{-13}	5.8×10^{-12}	Synthesis of prostaglandins and thromboxanes	0.004	0.623
Phospholipid synthesis	2.1×10^{-13}	5.9×10^{-12}	Synthesis of bile acids and bile salts via 24-hydroxycholesterol	0.025	0.623
Arachidonic acid metabolism	9.3×10^{-12}	1.8×10^{-10}	Chondroitin sulfate/dermatan sulfate metabolism	0.032	0.623
Methionine metabolism	1.0×10^{-10}	1.5×10^{-9}	Chondroitin sulfate/dermatan sulfate degradation	0.032	0.623
Lysine degradation	5.1×10^{-9}	4.8×10^{-8}	Hyaluronan metabolism	0.032	0.623
Biotin metabolism	5.1×10^{-9}	4.8×10^{-8}	Hyaluronan uptake and degradation	0.032	0.623
Pyruvate metabolism	8.1×10^{-9}	6.6×10^{-8}	Cellular responses to stress	0.037	0.623
Pentose phosphate pathway	4.3×10^{-8}	3.0×10^{-7}	Detoxification of reactive oxygen species	0.037	0.623
Histidine metabolism	4.8×10^{-8}	3.1×10^{-7}	Visual phototransduction	0.041	0.623
Glycerolipid metabolism	7.0×10^{-8}	4.0×10^{-7}	Diseases associated with visual transduction	0.041	0.623

[1]Pathway enrichment was based on a metabolite set enrichment analysis for metabolites and on a significance analysis of functional categories in gene expression analysis for gene transcripts. FDR, false discovery rate; SAT, subcutaneous adipose tissue; VAT, visceral adipose tissue.

correlated with BMI in both SAT and VAT. On the basis of the volume to surface area relation in adipocytes, we propose that the ratio between triglycerides and membrane lipids may constitute a novel approach for estimating adipocyte cell size as supported by microscopic image analysis (see Figure 2). Moreover, the abovementioned lipid ratio may constitute a more sensitive

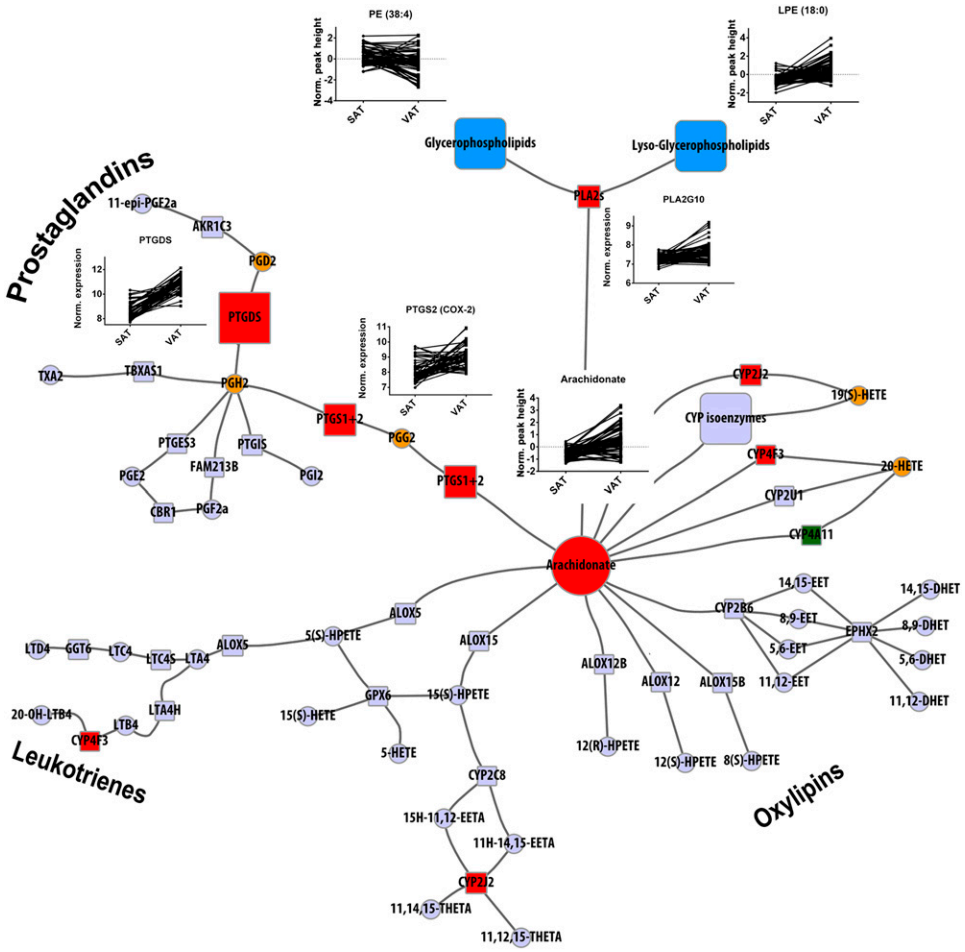

FIGURE 3 Biochemical network of arachidonic acid metabolism. Combined transcriptomic and metabolic network analysis of differences in arachidonic acid metabolism between VAT and SAT adipose tissues. Metabolites are illustrated as circles; genes are illustrated as squares. Significant (FDR <0.05) members of the network are colored red or green (higher or lower in VAT, respectively). Node size is proportional to fold change. No oxylipins, prostaglandins, or leukotrienes were measured in this study, but orange indicates a predicted alteration in abundances in VAT based on the combined measured metabolic network. Blue indicates a group of multiple metabolites being accepted as substrate/product. FDR, false discovery rate; LPE, lysophosphatidylethanolamine; PE, phosphatidylethanolamine; SAT, subcutaneous adipose tissue; VAT, visceral adipose tissue.

metric than BMI alone to identify limits of adipocyte storage capacity and to characterize obese phenotypes.

Differences in VAT lipids based on CRC tumor stage

Logistic regression adjusting for sex, age, tumor location, and BMI was used to identify lipids in both adipose tissues associated with CRC tumor stage, but none remained significant after FDR correction. However, several lipids showed trends with increasing tumor stage, based on Kendall's τ correlation (Figure 2A and Supplemental Table 4). These lipids may constitute potential biological markers of CRC progression that deserve further investigation. Unfortunately, these species' low abundance prevented their structure elucidation using tandem MS. Furthermore, their abundances in serum were below the instrumental limits of detection.

We generally observed limited correlations between adipose tissue and serum metabolites. This suggests that blood-based measurements of species analyzed by the current investigation have a limited value as surrogate markers of adipose tissue metabolism.

Integrated metabolomic and transcriptomic measurements suggest higher inflammatory signaling in VAT compared with SAT

Integrated analysis of SAT and VAT adipose gene expression and small-molecule gene end products (metabolites) suggest a greater inflammatory environment in VAT than in SAT. Arachidonic acid, a precursor for eicosanoid synthesis (e.g., series 2 prostaglandins) (Figure 3), was the only significantly elevated fatty acids in VAT compared with SAT. A recent case-control study identified an elevation in arachidonic acid in VAT of colon cancer patients (37). However, their analysis was limited by transmethylation derivatization, which precludes the decoupling of complex lipid esterified and free arachidonic acid abundances, which is required for biochemical network interpretations. Arachidonic acid is primarily bound in the sn-2 position of membrane phospholipids (phosphatidylcholine, phosphatidylethanolamine, ether lipids) and is released via phospholipase A2 activity (38). We observed lower concentrations of phosphatidylethanolamines, phosphatidylcholines, and plasmalogens [(phosphatidylethanolamine (38:4), phosphatidylethanolamine (P-38:4), phosphatidylcholine (P-16:0/20:4)], all of which putatively contain arachidonic acid (20:4). We also observed elevations in products of phospholipase activity, such as lyso-lipids [lysophosphatidylethanolamine (18:0), lysophosphatidylcholine (18:0)] in VAT than in SAT. Further gene expression analysis confirmed a higher *PLA2* expression in VAT than in SAT. Particularly, the *PLA2G10* isoform was significantly overexpressed in VAT and may directly contribute to the observed elevation in free arachidonic acid in this tissue. Although no eicosanoids and other oxylipins were measured in this study, we observed significantly higher gene expression for both *PTGDS* and *PTGS2* (also known as *COX2*) in VAT compared with SAT. On the basis of higher availability of free arachidonic acid and elevated gene expression for enzymes involved in inflammatory signaling, we hypothesize that compared with SAT, VAT produces elevated concentrations of inflammatory lipid signaling mediators, specifically prostaglandins G2, H2, and D2 (see Figure 3).

Evidence for the role of adipose tissue in endocrine and immunologic functions beyond lipid storage is increasing (39). On the basis of the current investigation of different adipose tissue compartments, we conclude that VAT is particularly metabolically active and may constitute an important source of organismal signaling lipid production (e.g., inflammatory mediators). However, it is important to mention that adipose tissue can be infiltrated with immune cells (40), particularly in obese individuals. Therefore, some of the aforementioned metabolic and transcriptomic changes between VAT and SAT may also stem from differences in cell types beyond adipocytes (e.g., infiltrating macrophages). Despite the potential effects of tissue heterogeneity, the observed inflammatory characteristics of VAT may help provide an additional link between visceral adiposity and carcinogenesis.

Strengths and limitations

The study design minimized patient-specific variance with paired sample collection of different adipose tissues compartments and serum. Advanced metabolomic and transcriptomic profiling techniques were used to measure an unprecedented number of metabolites and gene transcripts in VAT and SAT. Integrated transcriptomic and metabolomic data analyses were used to strengthen and corroborate metabolomic results. One limitation of this study is that conclusions can be drawn only on a "tissue" and not on a cell type–specific level. Thus, more detailed investigations will be needed to determine the potential impact of adipose tissue cell composition on its metabolic profiles. The study was designed to cast a wide metabolomic net to identify potentially affected species, which subsequently identified the need to conduct follow-up studies targeting for analyses of eicosanoids and other lipid signaling mediators as well as a bigger sample size to validate potential markers of CRC tumor stage.

In conclusion, our study comprehensively characterized the global metabolic differences of human adipose tissue compartments (visceral and subcutaneous) in a CRC context by using integrated metabolomic, lipidomic, and transcriptomic analyses. Although both adipose tissue types displayed fundamentally different metabolic profiles, VAT can be characterized as more metabolically active and contains higher abundances of most primary metabolites measured. Most important, VAT displayed elevated markers of inflammatory signaling, as evident by higher concentrations of arachidonic acid and elevated gene expression for phospholipases and enzymes involved in prostaglandin synthesis.

ColoCare study protocols, questionnaires, and procedures were developed in collaboration with the ColoCare Fred Hutchinson Cancer Research Center investigators. We thank our collaborators on the ColoCare recruitment, particularly Hermann Brenner, Jenny Chang-Claude, and Michael Hoffmeister. We are grateful to all the study staff who have made this study possible, especially Torsten Kölsch, Susanne Jakob, Clare Abbenhardt, Stefanie Zschäbitz, Werner Diehl, Rifraz Farook, Lin Zielske, Anett Brendel, Marita Wenzel and Renate Skatula. We thank the National Center for Tumor Diseases Tissue and Liquid Biobank for sample storage and handling as well as the microarray unit of the DKFZ Genomics and Proteomics Core Facility for providing the Illumina Whole-Genome Expression BeadChips and related services.

The authors' responsibilities were as follows—DBL, DS, OF, JWL, and CMU: designed the research; DBL, JFF, M Salou, and DS: performed the laboratory analyses; DS, NH, JB, PS-K, BG, M Schneider, AU, EH, PS, OF, and CMU: provided essential materials and resources; DBL, DG, JFF, and RT: analyzed the data and performed the statistical analyses; DBL, DS, NH, JWL, and CMU: assisted in the interpretation of the data; DBL, DG, JFF, DS, OF, JWL, and

CMU: wrote the manuscript; JWL and CMU: had primary responsibility for the final content; and all authors: read and approved the final manuscript. The authors declared that there were no conflicts of interest related to this study.

REFERENCES

1. Wu S, Liu J, Wang X, Li M, Gan Y, Tang Y. Association of obesity and overweight with overall survival in colorectal cancer patients: a meta-analysis of 29 studies. Cancer Causes Control 2014;25:1489–502.
2. van Kruijsdijk RC, van der Wall E, Visseren FL. Obesity and cancer: the role of dysfunctional adipose tissue. Cancer Epidemiol Biomarkers Prev 2009;18:2569–78.
3. Bastard JP, Maachi M, Lagathu C, Kim MJ, Caron M, Vidal H, Capeau J, Feve B. Recent advances in the relationship between obesity, inflammation, and insulin resistance. Eur Cytokine Netw 2006;17:4–12.
4. Ibrahim MM. Subcutaneous and visceral adipose tissue: structural and functional differences. Obes Rev 2010;11:11–8.
5. Fox CS, Massaro JM, Hoffmann U, Pou KM, Maurovich-Horvat P, Liu CY, Vasan RS, Murabito JM, Meigs JB, Cupples LA, et al. Abdominal visceral and subcutaneous adipose tissue compartments: association with metabolic risk factors in the Framingham Heart Study. Circulation 2007;116:39–48.
6. Pou KM, Massaro JM, Hoffmann U, Lieb K, Vasan RS, O'Donnell CJ, Fox CS. Patterns of abdominal fat distribution: the Framingham Heart Study. Diabetes Care 2009;32:481–5.
7. Denkert C, Bucher E, Hilvo M, Salek R, Oresic M, Griffin J, Brockmoller S, Klauschen F, Loibl S, Barupal DK, et al. Metabolomics of human breast cancer: new approaches for tumor typing and biomarker discovery. Genome Med 2012;4:37.
8. Ikeda A, Nishiumi S, Shinohara M, Yoshie T, Hatano N, Okuno T, Bamba T, Fukusaki E, Takenawa T, Azuma T, et al. Serum metabolomics as a novel diagnostic approach for gastrointestinal cancer. Biomed Chromatogr 2012;26:548–58.
9. Putluri N, Shojaie A, Vasu VT, Vareed SK, Nalluri S, Putluri V, Thangjam GS, Panzitt K, Tallman CT, Butler C, et al. Metabolomic profiling reveals potential markers and bioprocesses altered in bladder cancer progression. Cancer Res 2011;71:7376–86.
10. Liesenfeld DB, Habermann N, Owen RW, Scalbert A, Ulrich CM. Review of mass spectrometry–based metabolomics in cancer research. Cancer Epidemiol Biomarkers Prev 2013;22:2182–201.
11. Siegel EM, Ulrich CM, Poole EM, Holmes RS, Jacobsen PB, Shibata D. The effects of obesity and obesity-related conditions on colorectal cancer prognosis. Cancer Control 2010;17:52–7.
12. Scholz M, Fiehn O. SetupX—a public study design database for metabolomic projects. Pacific Symposium on Biocomputing Pacific Symposium on Biocomputing 2007:169–80.
13. Fiehn O, Wohlgemuth G, Scholz M, Kind T, Lee do Y, Lu Y, Moon S, Nikolau B. Quality control for plant metabolomics: reporting MSI-compliant studies. Plant J 2008;53(4):691–704.
14. Matyash V, Liebisch G, Kurzchalia TV, Shevchenko A, Schwudke D. Lipid extraction by methyl-tert-butyl ether for high-throughput lipidomics. J Lipid Res 2008;49:1137–46.
15. Weckwerth W, Wenzel K, Fiehn O. Process for the integrated extraction, identification and quantification of metabolites, proteins and RNA to reveal their co-regulation in biochemical networks. Proteomics 2004;4:78–83.
16. Fiehn O. Extending the breadth of metabolite profiling by gas chromatography coupled to mass spectrometry. Trends Anal Chem 2008; 27:261–9.
17. Kind T, Tolstikov V, Fiehn O, Weiss RH. A comprehensive urinary metabolomic approach for identifying kidney cancerr. Anal Biochem 2007;363:185–95.
18. Fiehn O, Wohlgemuth G, Scholz M. Setup and annotation of metabolomic experiments by integrating biological and mass spectrometric metadata. Lect Notes Comput Sci 2005;3615:224–39.
19. Fiehn O, Wohlgemuth G, Scholz M. Setup and annotation of metabolomic experiments by integrating biological and mass spectrometric metadata. In: Ludäscher B, Raschid L, editors. Data integration in the life sciences. Berlin (Germany): Springer; 2005. p. 224–39.
20. Pluskal T, Castillo S, Villar-Briones A, Oresic M. MZmine 2: modular framework for processing, visualizing, and analyzing mass spectrometry-based molecular profile data. BMC Bioinformatics 2010;11:395.
21. Eberwine J, Yeh H, Miyashiro K, Cao Y, Nair S, Finnell R, Zettel M, Coleman P. Analysis of gene expression in single live neurons. Proc Natl Acad Sci USA 1992;89:3010–4.
22. Johnson WE, Li C, Rabinovic A. Adjusting batch effects in microarray expression data using empirical Bayes methods. Biostatistics 2007;8: 118–27.
23. Du P, Kibbe WA, Lin SM. lumi: a pipeline for processing Illumina microarray. Bioinformatics 2008;24:1547–8.
24. Leek JT, Johnson WE, Parker HS, Fertig EJ, Jaffe AE, Storey JD. sva: Surrogate Variable Analysis. 3.14.0. ed. 2014.
25. van den Berg RA, Hoefsloot HC, Westerhuis JA, Smilde AK, van der Werf MJ. Centering, scaling, and transformations: improving the biological information content of metabolomics data. BMC Genomics 2006;7:142.
26. Xia J, Mandal R, Sinelnikov IV, Broadhurst D, Wishart DS. MetaboAnalyst 2.0—a comprehensive server for metabolomic data analysis. Nucleic Acids Res 2012;40:2.
27. Benjamini Y, Hochberg Y. Controlling the false discovery rate: a practical and powerful approach to multiple testing. J R Stat Soc B 1995;57:289–300.
28. Grapov D, Fahrmann J, Hwang J, Poudel A, Jo J, Periwal V, Fiehn O, Hara M. Diabetes associated metabolomic perturbations in NOD mice. Metabolomics 2015;11:425–37.
29. Kanehisa M, Goto S, Sato Y, Furumichi M, Tanabe M. KEGG for integration and interpretation of large-scale molecular data sets. Nucleic Acids Res 2012;40:D109.
30. Barry WT, Nobel AB, Wright FA. Significance analysis of functional categories in gene expression studies: a structured permutation approach. Bioinformatics 2005;21:1943–9.
31. Barry W. safe: Significance Analysis of Function and Expression. 3.6.1 ed. 2014.
32. Croft D, Mundo AF, Haw R, Milacic M, Weiser J, Wu G, Caudy M, Garapati P, Gillespie M, Kamdar MR, et al. The Reactome pathway knowledgebase. Nucleic Acids Res 2014;42:D472–7.
33. Felländer G, Nordenstrom J, Tjader I, Bolinder J, Arner P. Lipolysis during abdominal surgery. J Clin Endocrinol Metab 1994;78:150–5.
34. Honsho M, Asaoku S, Fujiki Y. Posttranslational regulation of fatty acyl-CoA reductase 1, Far1, controls ether glycerophospholipid synthesis. J Biol Chem 2010;285:8537–42.
35. Wallner S, Schmitz G. Plasmalogens the neglected regulatory and scavenging lipid species. Chem Phys Lipids 2011;164:573–89.
36. Braverman NE, Moser AB. Functions of plasmalogen lipids in health and disease. Biochim Biophys Acta 2012;1822:1442.
37. Giuliani A, Ferrara F, Scimo M, Angelico F, Olivieri L, Basso L. Adipose tissue fatty acid composition and colon cancer: a case-control study. Eur J Nutr 2014;53:1029–37.
38. Piomelli D. Arachidonic acid in cell signaling. Curr Opin Cell Biol 1993;5:274–80.
39. Greenberg AS, Obin MS. Obesity and the role of adipose tissue in inflammation and metabolism. Am J Clin Nutr 2006;83:461S–5S.
40. Curat CA, Wegner V, Sengenes C, Miranville A, Tonus C, Busse R, Bouloumie A. Macrophages in human visceral adipose tissue: increased accumulation in obesity and a source of resistin and visfatin. Diabetologia 2006;49:744–7.